Fuel Processing Technology 213 (2021) 106712

Contents lists available at ScienceDirect

Fuel Processing Technology

journal homepage: www.elsevier.com/locate/fuproc

The microscopic oxidation mechanism of NH_3 on CuO(111): A first-principles study

Chaohe Zheng, Haibo Zhao *

State Key Laboratory of Coal Combustion, Huazhong University of Science and Technology, Wuhan 430074, PR China

ARTICLE INFO

Keywords:
Chemical looping
Selective catalytic reduction
Density functional theory
Copper oxide
Ammonia

ABSTRACT

Understanding the oxidation of ammonia (NH_3) over CuO surface and then the formation routes of N_2 and NO_x is rather crucial to provide a favorable direction for the rational design of high-performance Cu-based oxygen carriers in chemical looping combustion (CLC) and CuO-containing catalysts in selective catalytic reduction (SCR). This study aims to investigate the reaction mechanisms of nitrogen-containing species using density functional theory (DFT) calculations. The potential dehydrogenation pathway is identified as $NH_3^* \rightarrow NH_2^* + H^* \rightarrow NH(1)^* + 2H^* \rightarrow N(2)^* + 3H^*$, and the rate-determined step is the NH_2^* dehydrogenation. Additionally, we consider 10 dominating elementary reactions for the formation of N_2, NO, NO_2 and N_2O; two skeletal schemes of the NH_3 oxidation under low or high temperature conditions are then proposed. Under the low temperature condition of SCR, the majority of gaseous N_2 comes from the Eley–Rideal reaction between NH_2^* fragment and gaseous NO, while the lateral recombination of N* to form N_2 might play a more crucial role under the high temperature condition of CLC. The high temperature and surface adsorbed oxygen provide positive impacts on the yield of gaseous NO and NO_2, respectively. Finally, the effects of O_2 and H_2O on the fate of nitrogen during heterogeneous reactions have also been determined.

1. Introduction

In response to the global warming issues, Chemical Looping Combustion (CLC) [1–3] has been proposed as a promising and efficient technique for the utilization of fossil fuels with the characteristics of intrinsic CO_2 separation. In a CLC system, oxygen carrier (OC) is well-accepted as a key component to bridge the air reactor (AR) and the fuel reactor (FR). Cu-based OC materials have been recognized as promising OC candidates for chemical looping with oxygen uncoupling (CLOU) due to its excellent reactivity, relatively low cost, and high oxygen release rate under the O_2-deficient atmosphere. The reaction performances of Cu-based materials, *i.e.*, copper ores [4–6] and synthesized materials [7–10], have been widely tested in the CLC processes these years.

As for coal, a cheaper and more abundant solid fuel, there are quite a number of opportunities and challenges remained in the CLC of coal, and China has become the main research battlefield recently [11,12]. As known, although the thermal-NO_x and prompt-NO_x can be inhibited in the CLC process, fuel nitrogen in coal will inevitably facilitate the formation of NO_x (including NO, NO_2 and N_2O) [13,14]. These formed NO_x compounds release as impurities in FR outlet, which influence the subsequent compression, transport and storage of CO_2 and even become vital precursors of acid rain [15–17].

The NH_3 formation during the pyrolysis and gasification of coal has been investigated for a long time [18–25]. Li et al. [18–21] proposed that the hydrogenation of nitrogen in solid char-N was the main route for the formation of NH_3. In terms of the type and relative level of released nitrogen volatiles, a general opinion is that the considerable NH_3 is mainly produced from fuels of lower-rank coal and biomass [23,24]. The intermediates of NH_3 are accepted as the main nitrogen precursors, which can be further oxidized by the OC particles *via* the complex gas-solid heterogeneous reactions to produce non-negligible gaseous NO_x compounds [13,17,24,26,27]. Therefore, a fundamental understanding of the NO_x formation from the NH_3 oxidation is highly desired.

These years, many investigations have been attempted to provide a comprehensive overview of heterogeneous reactions that take place between N-containing species and OCs in a CLC process. During the process of *in-situ* gasification CLC (*i*G-CLC) of coal, most nitrogen species in coal are converted as gaseous N_2, and minor amounts of NO could be produced [27,28]. When using a CuO-based OC in a CLOU process of

* Corresponding author.
E-mail address: hzhao@mail.hust.edu.cn (H. Zhao).

https://doi.org/10.1016/j.fuproc.2020.106712
Received 14 October 2020; Received in revised form 4 December 2020; Accepted 12 December 2020
Available online 21 December 2020

coal, Song et al. [13] found that NO together with less NO_2 and N_2O was generated. Pérez-Vega et al. [17] concluded that most of the fuel-nitrogen was reduced to produce N_2, while about 20 wt% of nitrogen was released in the form of NO in CLOU. Normann et al. [24] demonstrated that under most of the CLOU conditions, CuO oxygen carrier was able to thoroughly convert NH_3 into NO or N_2, with considerable amounts of NO_x. However, the comprehensive oxidation process of N-containing species under the high temperature conditions of CLC is not entirely clear.

In addition, to control the NO_x emission, selective catalytic reduction (SCR) has been regarded as the most effective de-NO_x technology these years [29–31]. And in the field of the NH_3-SCR, a suitable catalyst with a high de-NO_x catalytic activity and low working temperature window (200 °C or even lower) is rather desired. Among all potential catalysts, CuO-based catalysts, *i.e.*, CuO/γ-Al_2O_3, CuO/TiO_2, *etc*, have been deemed as promising candidates due to its high de-NO_x performance and exquisite coordinative flexibility in the low working temperature range [32–38]. Since the slight addition or doping of appropriate amount of CuO into metal oxides can bring a higher low-temperature catalytic property, a series of publications thus focused on searching potential copper-containing catalysts, and then attempted to analyze the reasons for the excellent NH_3-SCR activity of their catalysts recently [39–43]. These two years, it was still principally attributed to the good dispersion of the active ingredient of CuO [39,40]. Qi et al. [41] and Wang et al. [42] emphasized the Lewis acid sites on the catalyst surface significantly influenced adsorption of NO_x and NH_3. However, they were mainly based on the common macroscopic observations, with a lack of the intrinsic characteristics of CuO itself. Accordingly, the comprehensive understanding of intrinsic reaction mechanism of NH_3 and its by-products over CuO surface is urgently required, which might be significantly beneficial to determine the synergistic effect of the components or even develop a suitable CuO-containing catalyst in the NH_3-SCR technology.

With the rapid development of density functional theory (DFT) these years, DFT method has become a more and more popular computing tool to successfully provide atomic level insights into the interaction between NH_3 molecule and various substrate models [44–50]. Shojaee et al. [45,46] systemically proposed the formation paths of gaseous N_2, NO and N_2O derived from the ammonia decomposition on Co_3O_4 surface, and Yang et al. [48] investigated the oxidation of ammonia and then raised potential formation pathways of N_2, NO, NO_2 and N_2O over $CuMn_2O_4$(100) surface, both of which were really helpful to understand the gas-solid heterogeneous reactions that take place between OCs and gaseous NH_3 molecule. However, to our knowledge, there is no such research on the oxidation of ammonia over CuO surface, which significantly limits the fundamental insights into the nitrogen evolution in both the CLC and SCR processes.

Thus, in this study, DFT calculations are applied to explore the successive dehydrogenations and further oxidation mechanism of NH_3, including exploring the active adsorption sites of NH_3 and its resultant dissociated products (*e.g.*, NH_2, NH, and N), the dehydrogenation pathways of NH_3 over CuO(111) surface, and the fate of nitrogen that reflects the formation pathways of N_2, NO, N_2O, and NO_2. The framework is as follows: the modeling parameters and computational details of our study is introduced in Section 2. Then, in Section 3.1, the adsorptions of N-containing species are primarily explored. Based on the above adsorption results, the stepwise dehydrogenations of NH_3 molecule are determined in Section 3.2. The several formation routes of N_2, NO, N_2O and NO_2 during the homogeneous and heterogeneous reactions between N-containing species are shown in Section 3.3. Finally, two skeletal schemes of the NH_3 oxidation under low or high temperature conditions are thus concluded in Section 3.4.

2. Computational details

All the DFT calculations are performed using the generalized gradient approximation (GGA) by the program of CASTEP (Cambridge Serial Total Energy Package) [51]. The Perdew-Wang (PW91) with an energy cutoff of 400 eV is conducted for the electron exchange-correlation energy [52]. The ultra-soft pseudo-potential is chosen to describe the electron-ion interactions. In terms of the GGA + U method, the Hubbard parameter of 7.5 eV is set to well deal with the strong electron correlations for the Cu 3d orbitals [53]. The van der Waals-inclusive correction (DFT-D) raised by the Ortmann, Bechstedt, and Schmidt (OBS) is applied in this study. In this calculations, the lattice parameters of the CuO cell ($a = 4.653$ Å, $b = 3.410$ Å, $c = 5.108$ Å, and $\beta = 99.50°$) are in good agreement with experimental values ($a = 4.682$ Å, $b = 3.424$ Å, $c = 5.127$ Å, and $\beta = 99.42°$) [54]. The six-layer p (2 × 3) CuO(111) slab, the most stable low-index CuO surface that contains compact Cu-O layers, is constructed with the bottom three layers fixed [55,56], and the vacuum space is 15 Å. The Monkhorst-Pack mesh for the surface calculations is chosen as 3 × 2 × 1. The convergence criterion for the total energy is 1.0×10^{-5} eV/atom, and the maximum interatomic force and displacement are set as 0.03 eV/Å and 0.001 Å. More details of corresponding modeling can refer to our previous studies [56,57]. The adsorption energy (E_{ads}) is expressed as:

$$E_{ads} = E(AB) - E(A) - E(B) \quad (1)$$

where E(AB), E(A), and E(B) represent the total energies of the adsorption structure, the substrate, and the adsorbate. For the energy barrier calculations, the transition state is calculated by the linear/quadratic synchronous transit (LST/QST) method. The energy barrier (E_b) is calculated as:

$$E_b = E(TS) - E(IS) \quad (2)$$

where E(TS) and E(IS) are the total energies of the transition state and the initial state, respectively.

3. Results and discussions

3.1. Adsorption of NH_x species

In order to determine the stable adsorption configurations of these molecules on the CuO(111) surface, we consider two placement orientations (horizontal or vertical) and nine classical adsorption sites: three-coordinated oxygen top site (T_{O3f}), four-coordinated oxygen top site (T_{O4f}), three-coordinated copper top site (T_{Cu3f}), four-coordinated copper top site (T_{Cu4f}), bridge site between two three-coordinated oxygen atoms ($B_{O3f\text{-}O3f}$), bridge site between two three-coordinated copper atoms ($B_{Cu3f\text{-}Cu3f}$), bridge site between two four-coordinated oxygen atoms ($B_{O4f\text{-}O4f}$), bridge site between two four-coordinated copper atoms ($B_{Cu4f\text{-}Cu4f}$), and bridge site between three-coordinated copper and oxygen atoms ($B_{Cu3f\text{-}O3f}$). After geometric optimization, the optimized adsorption configurations of all molecules are depicted in Fig. 1, while the corresponding adsorption energies are listed in Table 1, respectively.

3.1.1. Adsorption of NH_3

Among all the adsorption configurations, it can be found that the structure where NH_3 is parallel to the T_{Cu3f} site is the optimal adsorption configuration. The adsorption energy of this adsorption configuration is −151.74 kJ/mol, and the equilibrium distance of Cu—N bond is 1.995 Å (Fig. 1a), which are similar with the results of NH_3 adsorption (−138.93 ~ −169.80 kJ/mol and 1.97– 2.03 Å) on the CuO/Al_2O_3 surface [58]. In addition, the bond length of N—H bond (1.010 Å) of free NH_3 molecule is slightly shorter than that of adsorbed NH_3, implying that the adsorption on the CuO surface weakens the interaction between H atoms and N atom, that is, the adsorption of NH_3 might promote its own dehydrogenation to some extent.

3.1.2. Adsorption of NH_2

Results demonstrate that the $B_{Cu3f\text{-}Cu3f}$ site is the most active site for

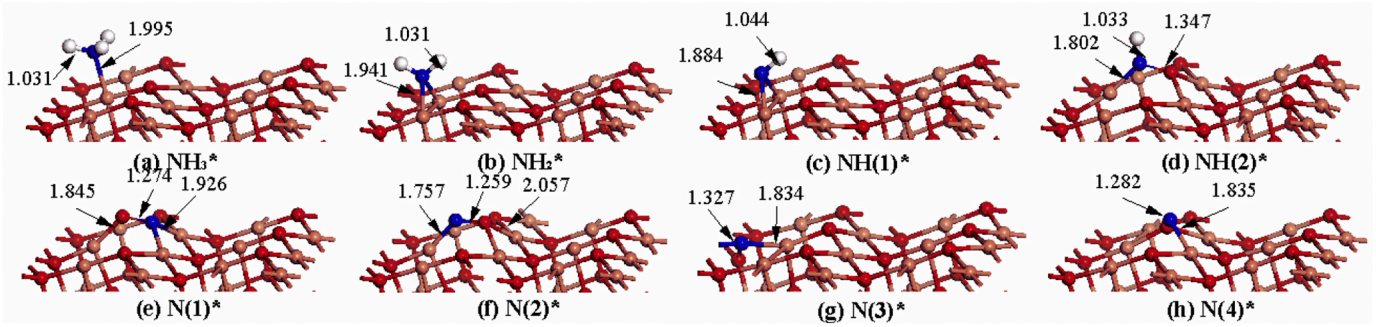

Fig. 1. The optimized geometric structures of NH_3*, NH_2*, NH*, and N* adsorptions on the CuO(111) surface, and '*' represents the adsorbed state. (Blue ball: N, White ball: H, Red ball: O, Salmon pink ball: Cu). (For interpretation of the references to colour in this figure legend, the reader is referred to the web version of this article.)

Table 1
The adsorption energy of NH_3*, NH_2*, NH*, and N* adsorptions.

Model	E_{ads}/kJ·mol^{-1}	Model	E_{ads}/kJ·mol^{-1}
NH_3*	−151.74	N(1)*	−682.15
NH_2*	−353.77	N(2)*	−622.93
NH(1)*	−451.75	N(3)*	−615.06
NH(2)*	−446.98	N(4)*	−596.22

NH_2* adsorption, and its adsorption energy is −353.77 kJ/mol. As shown in Fig. 1b, the bond lengths of the H—N bond and Cu—N bond are 1.031 Å and 1.941 Å, respectively. Different from the NH_3 adsorption in Fig. 1a, the nitrogen atom of NH_2* is converted to bond with double Cu atoms, and the Cu—N bond length also decreases from 1.998 Å to 1.941 Å. Namely, the interaction between N atom and Cu atoms is quite stronger, which well explains the remarkable increase of the adsorption energy.

3.1.3. Adsorption of NH

It is noted that NH* possesses two possible optimal adsorption configurations, which are parallel to the $B_{Cu3f\text{-}Cu3f}$ site (Fig. 1c) and perpendicular to the $B_{Cu3f\text{-}O3f}$ site (Fig. 1d). The corresponding adsorption energies of these two geometric structures are −451.75 kJ/mol and −446.98 kJ/mol, respectively. To dertermine the potential dehydrogenation pathway of the NH_2* fragment, both of the adsorption configurations are considered, and then the activation free energies of these two dehydrogenation pathways are calculated.

3.1.4. Adsorption of N

Although there are numerous initial geometric structures of N atom on the surface of CuO, the majority of surface structures will eventually generate four similar geometric configurations. Fig. 1(e–h) show these four stable adsorption configurations, and the adsorption energies are −682.15 kJ/mol, −622.93 kJ/mol, −615.06 kJ/mol, −596.22 kJ/mol, respectively. Analogously, these four geometric configurations of N atom will be set as the final dissociated products of NH* dehydrogenation to identify the most probable dissociation pathway.

3.2. Successive dehydrogenation of NH_3

To characterize the interaction between NH_3 and CuO, it is rather essential to explore the successive dehydrogenation process of NH_3 (NH_3* → NH_2* + H* → NH* + 2H* → N* + 3H*). According to the above adsorption configurations of NH_2*, NH*, and N*, the lowest energy co-adsorption configurations of NH_2* + H*(Fig. 3a), NH* + H* (Fig. 3(b–c)), and N* + H*(Fig. 3(d–g)) are constructed, which are set as the stepwise dehydrogenation products of NH_3*, NH_2*, and NH* species, respectively. The potential energy profiles of the NH_3 dehydrogenation paths are shown in Fig. 2, and the geometric structures are depicted in Fig. 3. Since hydrogen atom can be easily consumed by generating water

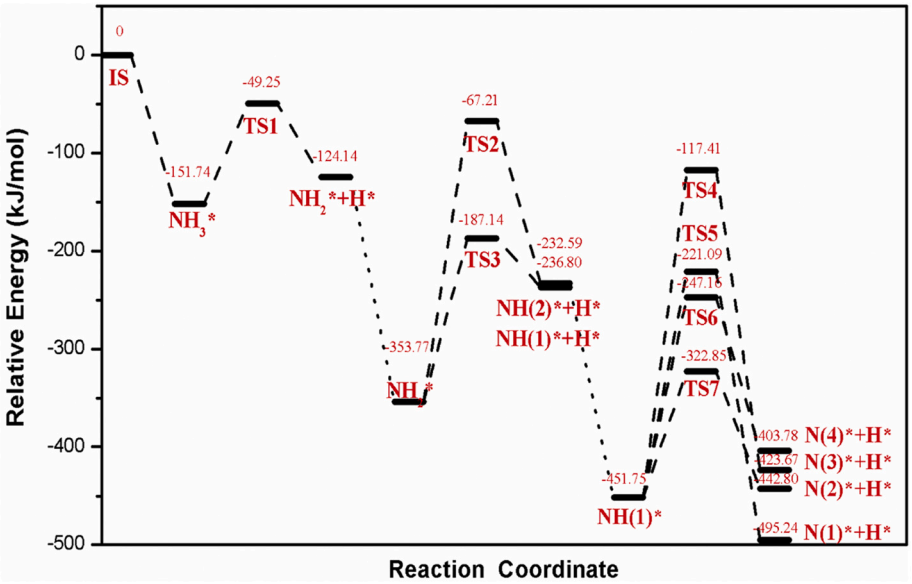

Fig. 2. Potential energy profiles of NH_3* dehydrogenation on the CuO surface.

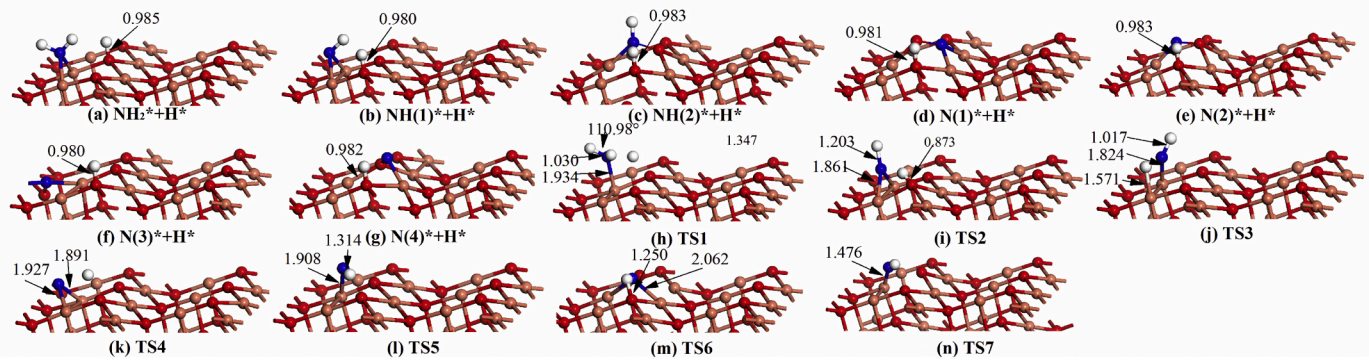

Fig. 3. The corresponding structures of NH_3* dehydrogenation on the CuO surface.

on the CuO surface [46,56], here we mainly focus on the reaction of the nitrogen-containing species, instead of the subsequent water formation.

As presented in Fig. 3a, NH_3* is liable to dissociate the first H atom (bonding with an adjacent tri-coordinated oxygen atom). Fig. 2 (TS1) shows the corresponding activation free energy of this reaction process. It is noted that the process of NH_3* → NH_2* + H* needs to overcome an energy barrier of 102.49 kJ/mol, and it is endothermic by 27.6 kJ/mol.

Fig. 2 (TS2) and (TS3) show the potential energy changes of the two different reaction paths of NH_2* → NH* + H*. As the second H atom dissociates to the adjacent tri-coordinated oxygen site, the reaction energy barrier (166.63 kJ/mol) of NH_2* → NH(1)* + H* (represented by Fig. 2 (TS3)) is apparently lower than the energy barrier (286.56 kJ/mol) of NH_2* → NH(2)* + H* (represented by Fig. 2 (TS2)), indicating that the dehydrogenation path of NH_2* → NH(1)* + H* is energetically favorable. This might be explained as: after the loss of the first H atom, the structure of NH_2* is more similar to the adsorption of NH(1)*, indicating that there would be less bond cleavages, namely lower energy barrier, during the dehydrogenation path of TS3.

Similarly, Fig. 2 (TS4–7) describes four possible reaction pathways of the NH(1)* dehydrogenation, where TS4 stands for NH(1)* → N(3)* + H*, TS5 for NH(1)* → N(1)* + H*, TS6 for NH(4)* → N(1)* + H*, and TS7 for NH(1)* → N(2)* + H*. As the third H atom dissociates and then adsorbs at the T_{O3f} site, it can be found from Fig. 2 (TS4–7) that the reaction energy barrier of TS7 (128.90 kJ/mol) is much lower than that of TS4 (334.34 kJ/mol), or TS5 (230.66 kJ/ mol), or TS6 (204.59 kJ/ mol), which implies that N(2)* is more probable to be the dissociated product from the NH(1)* dehydrogenation. At the same time, it is noted that the reaction heat of this path of NH(1)* → N(2)* + H* is slightly endothermic (8.95 kJ/mol), and the overall energy of N(2)* + H* is not the lowest. Namely, this implies that, when searching for transition states based on the principles of lowest energy, the most stable thermodynamic structure might not be the optimal kinetic reaction product. This is because the nitrogen atom in NH(1)* still bonds with the activated original Cu atom (the Cu—N bond length is 1.476 Å, see Fig. 3 (TS7)). Compared with other three pathways, the transition state of TS7 leads to less bond cracks, and the activation energy required for the dehydrogenation reaction is thus able to be sharply reduced. Additionally, the NH(1)* fragment has the lowest (1.044 Å) N—H bond length among three NH_x species, indicating that the bond energy of N—H bond is lower (the higher activation degree) than that of NH_2* or NH_3*, and the lower energy for further dehydrogenation is required.

In summary, the overall energy of reactants, transition states, and products (as shown in Fig. 2) are all negative, *i.e.*, below the overall energy of gaseous ammonia, which implies that NH_3* is prone to undergo consecutive dehydrogenations to N* rather than the desorption from the CuO surface, which is similar with the previous results [46,48]. The optimal dehydrogenation pathway of NH_3* molecule over CuO surface is NH_3* → NH_2* + H* → NH(1)* + 2H* → N(2)* + 3H*, and the rate-determined elementary step is identified as the NH_2* dehydrogenation (NH_2* → NH(1)* + H*).

3.3. The fate of nitrogen

In this section, the formation routes of nitrogen-containing products (NO, N_2, N_2O and NO_2) during the oxidation of NH_3 are investigated. By combining the potential reaction pathways of N_2, NOx formation in previous papers [45–48], we choose 10 typical dominating elementary reactions of N_2, NO, NO_2 and N_2O formation. As listed in Table 2, R1-R4 represent the formation paths of N_2, and Fig. 4 presents their energy barriers obtained by the transition state search. Analogously, the corresponding energy profiles of R5-R10 for the NO_x formation are shown in Fig. 6, and the energy profiles and microscopic configurations of different reaction paths are marked with six different colored lines and fonts.

3.3.1. The formation of N_2

The red line in Fig. 4 represents a common N_2 formation pathway of N* + N* → NN* → N_2* → N_2(g), which implies the recombination of two N* atoms (derived from the successive NH_3 dehydrogenations) to form N_2. Combining the energy barrier diagrams in Fig. 4(R1) and the configurations in Fig. 5(R1), it is observed that the recombination reaction of two adjacent N* to form a N*N* structure is spontaneously exothermic by 151.83 kJ/mol. Thus, the nitrogen-containing species, especially for surface N*, are not prone to stay in the surface to gradually produce metal nitrides, suggesting that the nitridation degree of the CuO surface is usually not too high. In addition, the N*N* structure can generate a N_2* structure by overcoming an energy barrier of 137.97 kJ/mol. This process is accompanied by the heat release of 167.76 kJ/mol, which means that this reaction is still liable to occur thermodynamically.

Additionally, we explore another N_2 generation pathway *via* the decomposition of N_2O molecule: N_2O* + $*^V$ → N_2* + O* → N_2(g), where "$*^V$" represents a surface oxygen vacancy. As seen in Fig. 5(R2), when gaseous N_2O molecule is adsorbed at a surface oxygen vacancy, the O atom (of N_2O molecule) will directly fill in the vacancy and then restore

Table 2
The reaction equations of N_2 and NO_x formation. ("$*^V$" represents a surface oxygen vacancy).

Species	Reaction Equation	No.
N_2 formation	N* + N* → NN* → N_2* → N_2(g)	R1
	N_2O* + $*^V$ → N_2* + O* → N_2(g)	R2
	NH_2* + NO(g) → N_2* + H_2O* → N_2(g) + H_2O*	R3
	NH* + NO(g) → N_2* + OH → N_2(g) + OH*	R4
NO formation	N* + Lattice O* → NO* → NO(g)	R5
NO_2 formation	NO* + Lattice O* → NO_2* → NO_2(g)	R6
	NO* + adsorbed O* → NO_2* → NO_2(g)	R7
N_2O formation	NH_2* + NO(g) → N_2O* + OH* → N_2O(g) + OH*	R8
	NH* + NO(g) → N_2O* + H* → N_2O(g) + H*	R9
	N* + NO* → N_2O* → N_2O(g)	R10

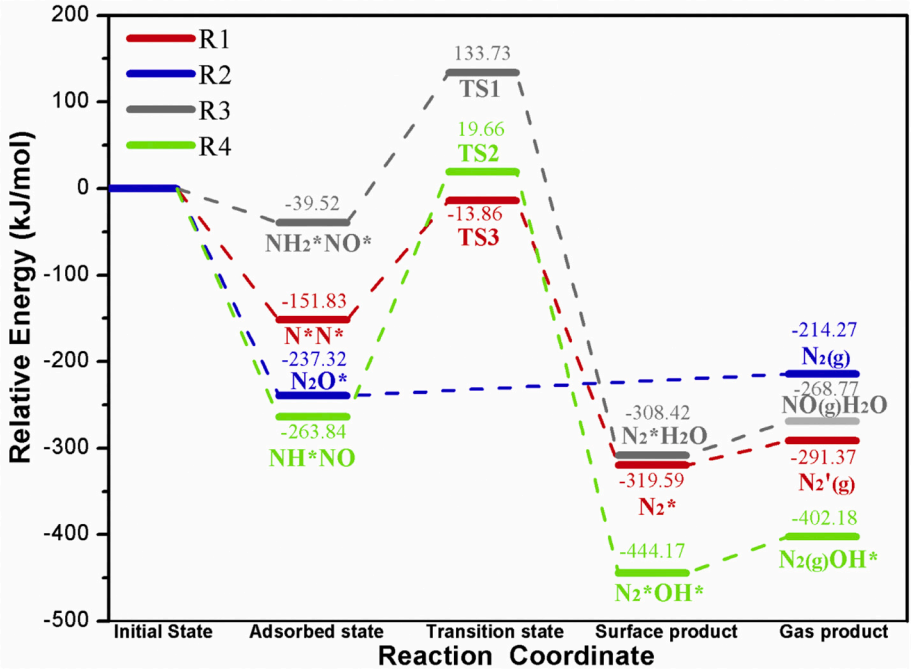

Fig. 4. Potential energy profiles of the formation routes of N_2 on the CuO surface.

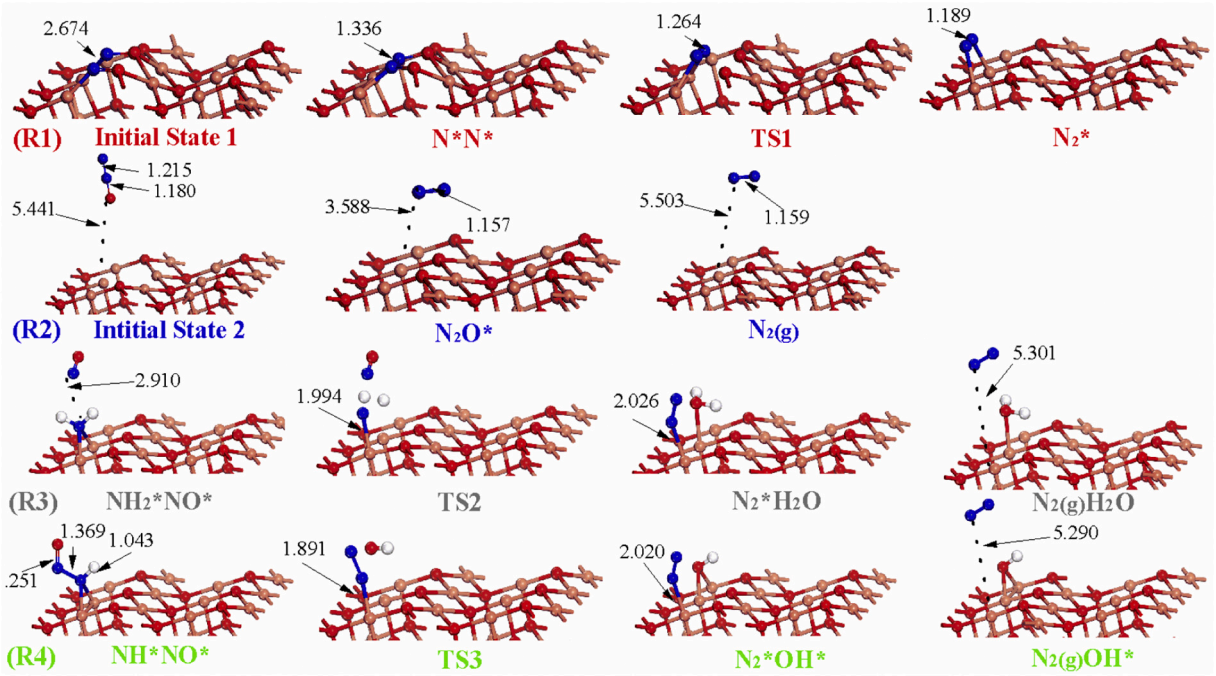

Fig. 5. The corresponding structures of the formation routes of N_2 on the CuO surface.

the CuO surface lattice oxygen, and spontaneously dissociate to form N_2*. This process is exothermic by 237.32 kJ/mol, and the desorption energy is only 23.05 kJ/mol.

The gray and green lines in Fig. 4 represent two typical formation pathways of gaseous N_2 in NH_3-SCR [48]: NH_2* + NO(g) → N_2* + H_2O* → N_2(g) + H_2O* and NH* + NO(g) → N_2* + OH* → N_2(g) + OH*. As depicted in Fig. 4(R3), the energy barrier of this N_2 formation path R3 is 173.25 kJ/mol, which is slightly higher than the energy barrier of the NH_2* dehydrogenation (166.63 kJ/mol), indicating that these two reactions should be on the same order of magnitude, and such a huge exothermic heat (268.90 kJ/mol) might provide the thermodynamic possibility to proceed this reaction as well. Nevertheless, the atomic interaction between NO and the adsorbed NH_2* is rather weak due to the physical adsorption (−39.52 kJ/mol), and the reactivity of this reaction is thus positively related to the concentration of NO and negatively related to temperature. Namely, this reaction under the low temperature condition is rather significant, and correspondingly the reactivity decreases as the temperature rises. Note that the reaction R3 showed in Fig. 5 is the heterogeneous reaction between gaseous NO and NH_2* *via* the Eley–Rideal mechanism, rather than the Langmuir–Hinshelwood mechanism. This is mainly because the energy barrier of the reaction between adsorbed NO* and NH_2* is calculated to be quite higher (above

500 kJ/mol) and the Langmuir–Hinshelwood reaction is thus not considered here, which well conforms to the experimental results obtained from *in situ* DRIFT spectra [41,42].

Furthermore, the reaction between NO and NH*, as depicted by NH*NO* in Fig. 5(R4), will first form a stable chemisorbed structure of (H-N-N-O)* group with a huge exothermic heat of 263.84 kJ/mol. This group can dissociate into N_2* and OH* by overcoming an energy barrier of 283.50 kJ/mol, with an apparent heat of 180.33 kJ/mol. The desorption energy of N_2 is 41.99 kJ/mol. However, the higher energy barrier (than that of NH* dehydrogenation) hints the kinetic difficulty of the reaction R4.

The above results mean that the recombination of two N* is not the only way for the formation of N_2, especially for the low temperature condition of SCR. This N_2-generation route is relatively dependent on the temperature, that is, with the increase of temperature, the reactivity of R1 increases correspondingly and the recombination reaction begins to play a more important role among all the N_2-formation routes. Comparatively speaking, the reaction R3 is recognized as the most potential NH_3-SCR path, and the reactivity of this reaction is negatively related to temperature due to the weak physisorption. Namely, this reaction under the low temperature condition is rather significant, and correspondingly the reactivity decreases as the temperature rises. In addition, the reactivity of the N_2O decomposition (R2) is relatively dependent on the concentrations of N_2O and oxygen vacancies, irrespective of the temperature. N_2O is able to easily dissociate into the oxygen vacancy under N_2O-rich and oxygen-deficient conditions, releasing N_2 and repairing the oxygen vacancy to form gaseous N_2 spontaneously.

3.3.2. *The formation of NO_x*

The red line in Fig. 6 represents the formation pathway of gaseous NO molecule: (R5) N* + Lattice O* → NO* → NO(g). The interaction between the surface N* and the adjacent lattice O* promotes the formation of NO*. As presented in Fig. 7(R5), the surface N* reacts with a lattice O* to form a (N—O)* group on the CuO surface, which will release as a gaseous NO with the creation of a surface oxygen vacancy. The rather low energy barrier (33.94 kJ/mol) suggests that the reaction is prone to occur kinetically. However, it must be noted that, although the NO* structure can be easily formed on the surface, the reaction heat required for the desorption process of NO* is 175.13 kJ/mol, which is recognized as the rate-limited elementary step of this reaction. At the same time, the adsorption and then decomposition of gaseous NO molecule on the defect surface is the inverse process of this reaction R5. The geometric configurations in Fig. 7(R5) NO* is the optimal adsorption site for gaseous NO molecule on the defect surface, and the adsorption energy is −175.13 kJ/mol. In other words, under the high reduction degree (or O_2-lean) condition (more oxygen vacancies exist in the surface), the NO molecule might be more likely to decompose its own oxygen atom to repair the oxygen defect. This is in good agreement with the experimental results that the NO generation rate decreases with the increase of the CuO reduction degree [24], which also clearly demonstrates the influence of the oxygen vacancies on the reactions of N*.

The blue and gray lines in Fig. 6 represent two NO_2 formation pathways: (R6) NO* + Lattice O* → NO_2* → NO_2(g) and (R7) NO* + adsorbed O* → NO_2* → NO_2(g), respectively. The former one means that NO is adsorbed on the CuO surface and then oxidized by a three-coordinated lattice O*, while the latter one represents the reaction between NO and a pre-adsorbed O* atom. It is noted that under the O_2-rich condition, the gas-phase O_2 molecule can easily adsorb on the defect surface and repair the oxygen vacancy to create a surface pre-adsorbed O* [59]. As presented in Fig. 7 (R7) (Initial State 1), one oxygen atom of the O_2 molecule fills into the vacancy, while another oxygen atom tends to adsorb at the $B_{Cu3f\text{-}Cu3f}$ site. It is found in Fig. 6 that the reactivity of the pre-adsorbed oxygen is extremely high, and the NO molecule can be oxidized to produce NO_2 molecule without an energy barrier; on the perfect surface, the activation energy of NO molecule to produce NO_2 molecule is 136.82 kJ/mol, and the desorption energy is 236.90 kJ/mol. Therefore, it is concluded that the CuO surface with the presence of abundant oxygen possesses a high catalytic activity for NO oxidation. In other words, both the presence of O_2 (R7) and high temperature (R6) will significantly promote the yield of NO_2 [13].

The green, black, and purple lines in Fig. 6 represent the N_2O formation pathways of R8-R10, *i.e.*, (R8) NH_2* + NO(g) → N_2O* + OH* → N_2O(g) + OH*, (R9) NH* + NO(g) → N_2O* + H* → N_2O(g) + H*, and (R10) NO* + N* → N_2O* → N_2O(g). That is, the gaseous NO reacts with the surface NH_2*, NH*, and N* to generate N_2O molecule, respectively. As shown in Fig. 6 (R8), the reaction energy barrier of R8 (257.62 kJ/

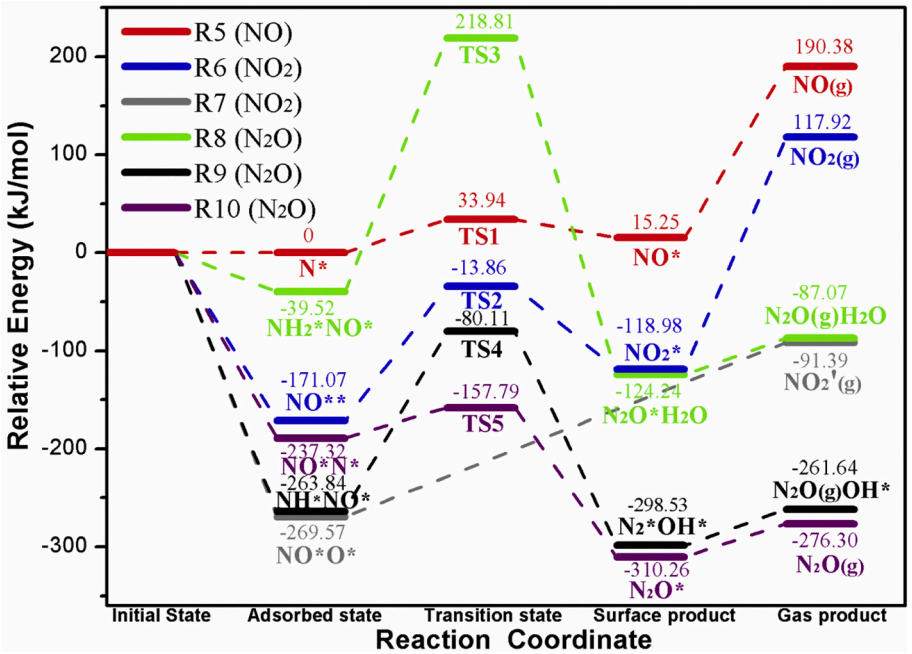

Fig. 6. Potential energy profiles of the formation routes of NO, NO_2 and N_2O on the CuO surface.

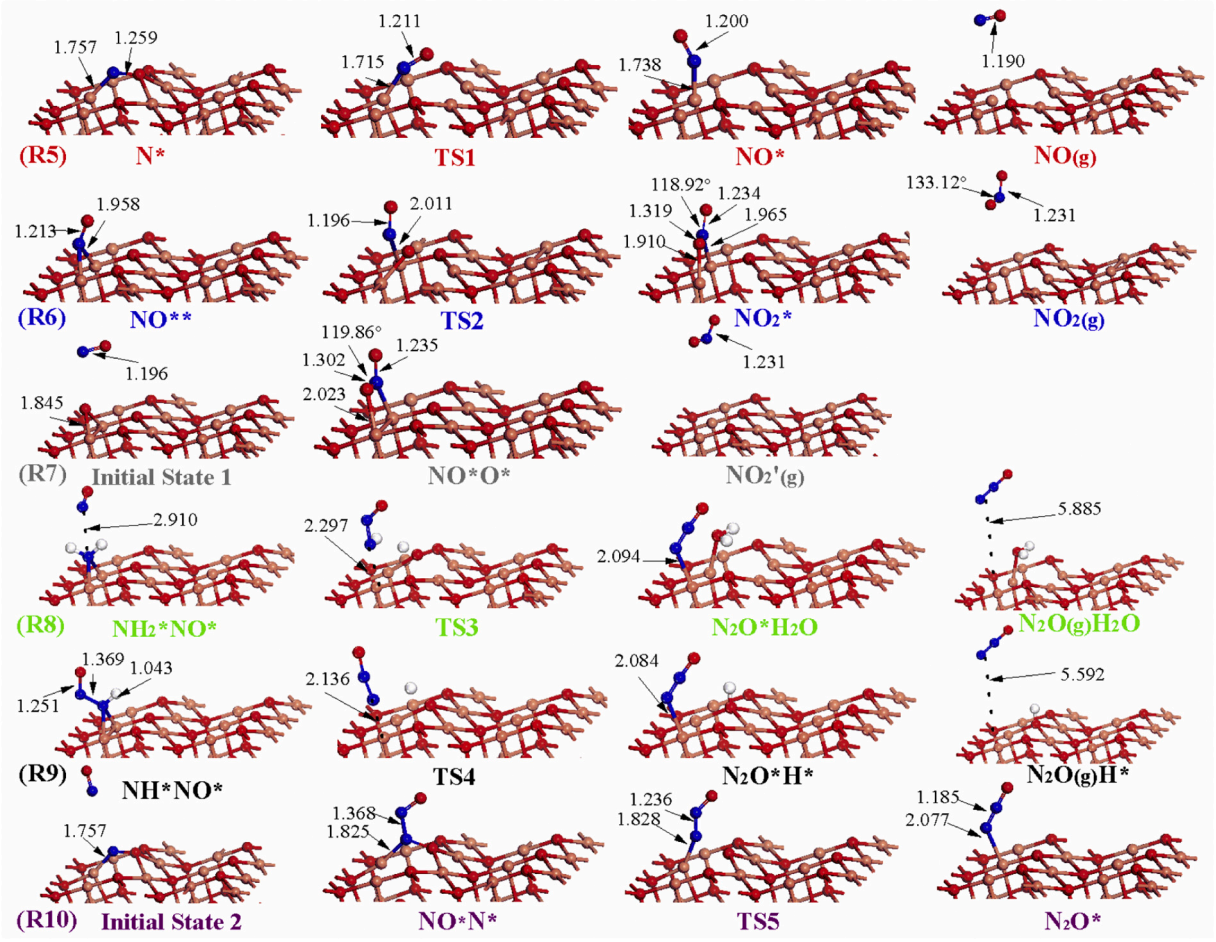

Fig. 7. The corresponding structures of the formation routes of NO, NO_2 and N_2O on the CuO surface.

mol) is significantly higher than that of R3 (173.25 kJ/mol) (to produce N_2), indicating that over the pure CuO surface, the Eley–Rideal reaction between NH_2* and gaseous NO is more likely to produce gaseous N_2, rather than gaseous N_2O. At the same time, it is noticed that the reaction energy barrier of R9 (183.73 kJ/mol) is significantly lower than that of R4 (283.50 kJ/mol), which implies that the reaction between NH* and NO is liable to produce gaseous N_2O. However, both energy barriers of R8 and R9 (as shown in Fig. 6) are quite higher than the energy barriers of the consecutive NH_3* dehydrogenations, indicating that the considerable N* would be produced during the whole process. Therefore, the N_2O formation derived from N* is rather essential. As depicted in Fig. 7 (R10), the gaseous NO molecule adsorbs on the N-containing surface to form a (N-N-O)* structure, which is slightly protruded far away from the surface. The low energy barrier (31.32 kJ/mol) and strong exothermicity (121.15 kJ/mol) indicate that the N_2O formation reaction R10 is rather easy to occur both kinetically and thermodynamically. In addition, the quite lower desorption energy (33.96 kJ/mol) also supports this inference. Briefly, the reaction R10 greatly

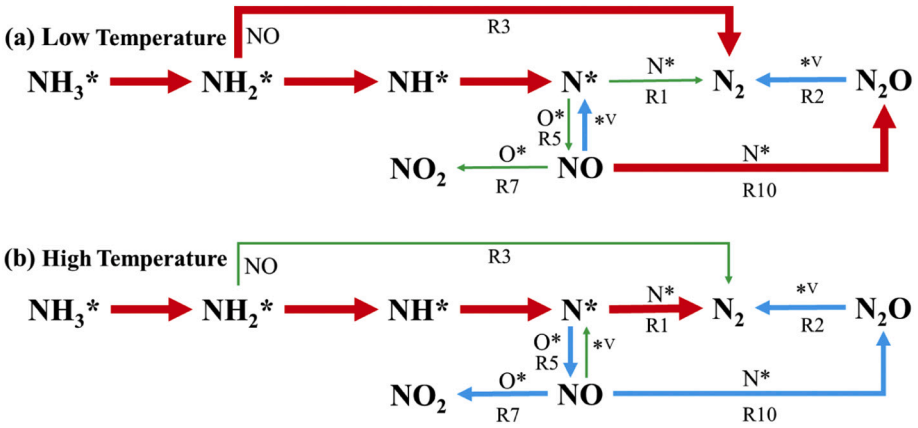

Fig. 8. Comprehensive nitrogen evolution over CuO surface under (a) low temperature (SCR) and (b) high temperature (CLC) conditions. (Red arrow: major contribution; Blue arrow: secondary contribution; Green arrow: minor contribution). (For interpretation of the references to colour in this figure legend, the reader is referred to the web version of this article.)

contributes to the generation of N_2O, while the reactions of R8-R9 contribute much less.

3.4. The overall nitrogen evolution

It is clear that over the CuO surface, NH_3 is liable to undergo three-step dehydrogenations ($NH_3^* \rightarrow NH_2^* \rightarrow NH^* \rightarrow N^*$) to form surface N*. Factually, some experiments have observed that N_2 and N_2O are the main products of NH_3 oxidation at low temperature, and the formation of NO (together with NO_2) at higher temperature becomes the preferred route of NO_x [24,41,42,60]. This trend can be well explained by the comprehensive nitrogen evolution shown in Fig. 8.

The recombination of two N* atoms to generate N_2 is prone to take place thermodynamically, suggesting that the nitridation degree of CuO surface is usually not too high. This is the reason why CuO always performs an excellent anti-nitrogen reactivity. However, considering the reaction routes of NOx formation, these reactions will consume a mass of the surface N* to some extent, and then obviously hinder the further recombination of N* to generate N_2, which might hint two rather different N-containing reaction mechanisms under low temperature or high temperature conditions, respectively.

At low temperature, although surface N* and lattice O* are easy to be activated due to the low activation energy (33.94 kJ/mol), the rather high desorption energy (175.13 kJ/mol) makes NO desorption rather difficult to occur (as indicated by Fig. 8a). That is, it is easier to exist in the form of adsorbed NO* or activated N* (the reverse reaction) at low temperature. These undesorbed NO* groups will react with surface N* to release gaseous N_2O molecule with a quite lower desorption energy of 33.96 kJ/mol; and activated N* remaining in the surface will also form N_2 through the recombination reaction, which also releases a large amount of heat (158.43 kJ/mol). However, as depicted in Fig. 4 and Fig. 8a, it has to be noted that the majority of gaseous N_2 might not derive from the lateral recombination of N*, but the decomposition of N_2O and the Eley–Rideal reaction between gaseous NO and NH_2*. The reaction R3 ($NH_2^* + NO(g) \rightarrow N_2^* + H_2O^* \rightarrow N_2(g) + H_2O^*$) is recognized as the most potential NH_3-SCR path at low temperature. The physisorption of gaseous NO and temperature sensitivity of this reaction convincingly support the arguments of the existing major problem of CuO-based catalysts in SCR (that is, the narrow working temperature window) [31]. Accordingly, to improve the temperature window of catalysts, a possible solution might be to strengthen the Eley–Rideal reaction between gaseous NO and adsorbed NH_2*. Namely, to utilize the synergistic effect of the components in CuO-based catalysts to elevate the adsorption ability of gaseous NO might become an effective way to promote the catalytic reduction ability of CuO-based catalysts.

Under high temperature condition of CLC, since high temperature can significantly promote the molecular thermal motion and the molecular desorption, surface N* and lattice O* are still easy to be activated to produce NO* group. These groups become quite easier to desorb to produce gaseous NO taking advantage of the molecular thermal motion, indicating that NO concentration is relevant to the temperature. Namely, the yield of NO in CLC becomes non-negligible [24]. NO will react with the three types of CuO surfaces (perfect, nitrogen-containing, and oxygen-containing surfaces) to generate gaseous N_2O and NO_2. The reactivity of these reactions will be accordingly promoted due to the significantly increased yield of gaseous NO at high temperature, decreasing the N_2O concentration and increasing the NO_2 concentration. As known, CuO begins to release gaseous O_2 under the CLOU temperature window (above 800 °C) [61], and these formed gaseous O_2 significantly contributes to the generation of gaseous NO_2 molecule (R7), which also well explains the reason why NO_2 concentration significantly increases in CLC. Furthermore, compared to the low temperature condition, the yield of N_2O decreases at high temperature, and with the progress of high-temperature reactions, a mass of surface oxygen defects will be inevitably produced and distinctly promote N_2O decomposition (R2), which well explains that the exhaust gas content of N_2O is detected not so high during a realistic CLC/CLOU process [13,17]. In addition, the recombination of two N* is correspondingly promoted by the increasing temperature. As indicated by Fig. 8b, the recombination reaction (R1) plays a more important role under high temperature condition of CLC when compared to the low temperature condition of SCR, and the decomposition of N_2O (R2) and the Eley–Rideal reaction between NO and NH_2* (R3) are inhibited to different extents.

Analogically, the reaction mechanisms in Fig. 8 can also explain the experimental observations that the presence of O_2 and H_2O will adversely affect the nitrogen evolution, *i.e.*, the decomposition of N_2O on the surface of the carriers [41,62,63]. On the one hand, both O_2 and N_2O exhibit a strong binding ability on the oxygen defect, and the decomposition of these two molecules will lead to the repair of the oxygen vacancy and the formation of by-products (the former one is adsorbed O*, and the latter one is N_2) [46]. On the other hand, the adsorptions of NO on the different surface sites (adsorbed O* and surface N*) possess an apparent competitive relationship. Therefore, the adverse effect of O_2 on nitrogen evolution includes that O_2 can not only directly react with nitrogen-containing species, but also be able to accelerate the restore of oxygen vacancies. Similarly, water molecule exhibits a high energetic affinity to the surface defect as well [64]. By repairing the oxygen vacancies on a reduced CuO surface, the adsorption and decomposition of O_2 and N_2O are thus inhibited. The former one might change the possible generation path of NO_2, while the latter one changes the formation routes of N_2O and N_2. Additionally, H_2O will also dissociate into an OH* radical as it adsorbs on the CuO surface, which might promote the NH_x dehydrogenations and heterogeneous reactions of NH_x to produce considerable N_2 or N_2O, thus helpfully illustrating how the nitrogen evolution is affected as H_2O is added to the inlet gas. Finally, particular attention in this paper is mainly paid on the interactions between the dehydrated NH_3 intermediates and stoichiometric CuO as well as the oxygen-covered surface and oxygen-defect surface, and the reactions between NH_3 and reduced copper species (Cu_2O, and/or Cu) might need further investigations [65,66].

4. Conclusions

The DFT studies are employed to investigate the oxidation of NH_3 to N_2 and NO_x (including NO, NO_2, and N_2O), and two skeletal schemes including the possible nitrogen evolution under low or high temperature conditions are proposed for NH_3 oxidation over CuO surface. The major conclusions are as follows:

(1) The optimal elementary reaction pathway of NH_3* dehydrogenation over CuO surface is identified as $NH_3^* \rightarrow NH_2^* + H^* \rightarrow NH(1)^* + 2H^* \rightarrow N(2)^* + 3H^*$, and the rate-determined elementary step is the secondary dehydrogenation of NH_2* ($NH_2^* \rightarrow NH(1)^* + H^*$).

(2) Under the low temperature condition, the Eley–Rideal reaction between NH_2* and gaseous NO is more likely to be the NH_3-SCR pathway to produce N_2, while the lateral recombination of N* might play a more crucial role under the high temperature condition of CLC.

(3) The Eley–Rideal reaction between gaseous NO and adsorbed NH_2* hints a narrow working temperature window, which is the major problem of CuO-based catalysts in SCR. One promising research direction is to promote the adsorption of gaseous NO *via* producing the synergistic effect of the components in CuO-based catalysts.

(4) The reactivity of the N_2O decomposition is relatively dependent on the concentrations of N_2O and oxygen vacancies, irrespective of the temperature. NO_2 is difficultly produced under the O_2-lean and low-temperature conditions, while the presence of both O_2 and high temperature can significantly promote the oxidation of NO.

(5) The negative effects of O_2 or H_2O on the N_2O decomposition are determined as the repair of the oxygen vacancy on the reduced CuO surface, with non-negligible by-products of adsorbed O* and OH* radicals.

Declaration of Competing Interest

The authors declare that they have no known competing financial interests or personal relationships that could have appeared to influence the work reported in this paper.

Acknowledgment

These authors were supported by “National Natural Science Foundation of China (51920105009, 52025063)”.

References

[1] J. Adanez, A. Abad, F. Garcia-Labiano, P. Gayan, L.F. de Diego, Progress in chemical-looping combustion and reforming technologies, Prog. Energy Combust. Sci. 38 (2) (2012) 215–282.
[2] H. Zhao, X. Tian, J. Ma, M. Su, B. Wang, D. Mei, Development of tailor-made oxygen carriers and reactors for chemical looping processes at Huazhong University of Science & Technology, Int. J. Greenh. Gas Con. 93 (2020) 102898.
[3] L. Yang, X. Wu, F. Liu, X. Zhang, J. He, K. Saito, Joint-use of activated carbon and carbon black to enhance catalytic stability during chemical looping methane decomposition process, Int. J. Hydrogen Energ. 45 (24) (2020) 13245–13255.
[4] Y. Wen, Z. Li, L. Xu, N. Cai, Experimental study of natural Cu ore particles as oxygen carriers in chemical looping with oxygen uncoupling (CLOU), Energy Fuel 26 (6) (2012) 3919–3927.
[5] Z. Gu, L. Zhang, C. Lu, S. Qing, K. Li, Enhanced performance of copper ore oxygen carrier by red mud modification for chemical looping combustion, Appl. Energy 277 (2020) 115590.
[6] Y. Wang, X. Tian, H. Zhao, K. Liu, The use of a low-cost oxygen carrier prepared from red mud and copper ore for in situ gasification chemical looping combustion of coal, Fuel Process. Technol. 205 (2020) 106460.
[7] I. Adánez-Rubio, A. Pérez-Astray, T. Mendiara, M.T. Izquierdo, A. Abad, P. Gayán, et al., Chemical looping combustion of biomass: CLOU experiments with a Cu-Mn mixed oxide, Fuel Process. Technol. 172 (2018) 179–186.
[8] J. Ma, D. Mei, W. Peng, X. Tian, D. Ren, H. Zhao, On the high performance of a core-shell structured CaO-CuO/MgO@AlO_3 material in calcium looping integrated with chemical looping combustion (CaL-CLC), Chem. Eng. J. 368 (2019) 504–512.
[9] I. Adánez-Rubio, S.T. Bararpour, A. Abad, P. Gayán, G. Williams, A. Scullard, et al., Performance evaluation of a Cu-based oxygen carrier impregnated onto ZrO_2 for chemical-looping combustion (CLC), Ind. Eng. Chem. Res. 59 (15, 2020) 7255–7266.
[10] X. Tian, M. Su, H. Zhao, Kinetics of redox reactions of CuO@TiO_2-Al_2O_3 for chemical looping combustion and chemical looping with oxygen uncoupling, Combust. Flame 213 (2020) 255–267.
[11] H. Zhao, X. Tian, J. Ma, X. Chen, M. Su, C. Zheng, et al., Chemical looping combustion of coal in China: comprehensive progress, remaining challenges, and potential opportunities, Energy Fuel 34 (6) (2020) 6696–6734.
[12] F. Liu, X. Wu, L. Yang, H. Bu, X. Zhang, Evaluation of a bauxite cement-bonded Fe-based oxygen carrier during a hundred of cycles under coal-fueled chemical looping combustion conditions, Fuel Process. Technol. 199 (2020) 106267.
[13] T. Song, W. Guo, L. Shen, Fuel nitrogen conversion in chemical looping with oxygen uncoupling of coal with a CuO-based oxygen carrier, Energy Fuel 29 (6) (2015) 3820–3832.
[14] H. Ge, L. Shen, H. Bai, S. Ma, S. Yin, P. Lu, et al., Characteristics of Zhundong coal ash in hematite-based chemical looping combustion, Energy Fuel 34 (7) (2020) 8150–8166.
[15] F. Normann, K. Andersson, B. Leckner, F. Johnsson, Emission control of nitrogen oxides in the oxy-fuel process, Prog. Energy Combust. Sci. 35 (5) (2009) 385–397.
[16] E. de Visser, C. Hendriks, M. Barrio, M.J. Mølnvik, G. de Koeijer, S. Liljemark, et al., Dynamis CO_2 quality recommendations, Int. J. Greenh. Gas Con. 2 (4) (2008) 478–484.
[17] R. Pérez-Vega, I. Adánez-Rubio, P. Gayán, M.T. Izquierdo, A. Abad, F. García-Labiano, et al., Sulphur, nitrogen and mercury emissions from coal combustion with CO_2 capture in chemical looping with oxygen uncoupling (CLOU), Int. J. Greenh. Gas Con. 46 (2016) 28–38.
[18] F. Tian, J. Yu, L.J. McKenzie, J. Hayashi, C. Li, Formation of HCN and NH_3 during the reforming of quinoline with steam in a fluidized-bed reactor, Energy Fuel 20 (1) (2006) 159–163.
[19] L. Tan, C. Li, Formation of NOx and SOx precursors during the pyrolysis of coal and biomass. Part I. effects of reactor configuration on the determined yields of HCN and NH_3 during pyrolysis, Fuel 79 (15, 2000) 1883–1889.
[20] L. Tan, C. Li, Formation of NOx and SOx precursors during the pyrolysis of coal and biomass. Part II. Effects of experimental conditions on the yields of NOx and SOx precursors from the pyrolysis of a victorian brown coal, Fuel 79 (15, 2000) 1891–1897.
[21] F. Tian, H. Wu, J. Yu, L. McKenzie, S. Konstantinidis, J. Hayashi, et al., Formation of NOx precursors during the pyrolysis of coal and biomass. Part VIII. Effects of pressure on the formation of NH_3 and HCN during the pyrolysis and gasification of victorian brown coal in steam, Fuel 84 (16, 2005) 2102–2108.
[22] J. Liu, X. Zhang, B. Hu, Q. Lu, D. Liu, C. Dong, et al., Formation mechanism of HCN and NH_3 during indole pyrolysis: a theoretical DFT study, J. Energy Inst. 93 (2) (2020) 649–657.
[23] P. Glarborg, A.D. Jensen, J.E. Johnsson, Fuel nitrogen conversion in solid fuel fired systems, Prog. Energy Combust. Sci. 29 (2) (2003) 89–113.
[24] F. Normann, M. Cheng, D. Zhao, Z. Li, N. Cai, H. Leion, Oxidation of ammonia over a copper oxide-containing solid oxygen carrier with oxygen uncoupling capability, Combust. Flame 165 (2016) 445–452.
[25] J. Liu, Q. Lu, X. Jiang, B. Hu, X. Zhang, C. Dong, et al., Theoretical investigation of the formation mechanism of NH_3 and HCN during pyrrole pyrolysis: the effect of H_2O, Molecules 23 (4) (2018) 711.
[26] J.E. Johnsson, Formation and reduction of nitrogen oxides in fluidized-bed combustion, Fuel 73 (9) (1994) 1398–1415.
[27] T. Song, L. Shen, J. Xiao, D. Chen, H. Gu, S. Zhang, Nitrogen transfer of fuel-N in chemical looping combustion, Combust. Flame 159 (3) (2012) 1286–1295.
[28] T. Mendiara, M.T. Izquierdo, A. Abad, L.F. de Diego, F. García-Labiano, P. Gayán, et al., Release of pollutant components in CLC of lignite, Int. J. Greenh. Gas Con. 22 (2014) 15–24.
[29] H. Chen, Y. Xia, H. Huang, Y. Gan, X. Tao, C. Liang, et al., Highly dispersed surface active species of Mn/Ce/TiW catalysts for high performance at low temperature NH_3-SCR, Chem. Eng. J. 330 (2017) 1195–1202.
[30] G. Qi, R.T. Yang, Low-temperature selective catalytic reduction of NO with NH_3 over iron and manganese oxides supported on titania, Appl. Catal. B-Environ. 44 (3) (2003) 217–225.
[31] L. Han, S. Cai, M. Gao, J.-y. Hasegawa, P. Wang, J. Zhang, et al., Selective catalytic reduction of NOx with NH_3 by using novel catalysts: state of the art and future prospects, Chem. Rev. 119 (19, 2019) 10916–10976.
[32] J.A. Sullivan, J.A. Doherty, NH_3 and urea in the selective catalytic reduction of NOx over oxide-supported copper catalysts, Appl. Catal. B-Environ. 55 (3) (2005) 185–194.
[33] J.H. Kwak, R. Tonkyn, D. Tran, D. Mei, S.J. Cho, L. Kovarik, et al., Size-dependent catalytic performance of CuO on γ-Al_2O_3: NO reduction versus NH_3 oxidation, ACS Catal. 2 (7) (2012) 1432–1440.
[34] H. Li, W. Zhang, J. Wang, Z. Yang, L. Li, K. Shih, Coexistence of enhanced Hg^0 oxidation and induced Hg^{2+} reduction on CuO/TiO_2 catalyst in the presence of NO and NH_3, Chem. Eng. J. 330 (2017) 1248–1254.
[35] C. Chen, Y. Cao, S. Liu, J. Chen, W. Jia, SCR catalyst doped with copper for synergistic removal of slip ammonia and elemental mercury, Fuel Process. Technol. 181 (2018) 268–278.
[36] L. Yang, Y. Jia, J. Cheng, X. Wu, J. He, F. Liu, Deactivation mechanism of activated carbon supported copper oxide SCR catalysts in C_2H_4 reductant, Can. J. Chem. Eng. 97 (10, 2019) 2708–2716.
[37] S. Yu, Y. Lu, F. Gao, L. Dong, Study on the crystal plane effect of CuO/TiO_2 catalysts in NH_3-SCR reaction, Catal. Today 339 (2020) 265–273.
[38] K. Kang, X. Yao, J. Cao, Z. Li, J. Rong, W. Luo, et al., Enhancing the K resistance of CeTiOx catalyst in NH_3-SCR reaction by CuO modification, J. Hazard. Mater. 402 (2021) 123551.
[39] H. Wang, B. Wang, J. Zhou, G. Li, D. Zhang, Z. Ma, et al., CuO modified vanadium-based SCR catalysts for Hg^0 oxidation and NO reduction, J. Environ. Manag. 239 (2019) 17–22.
[40] X. Wu, H. Meng, Y. Du, J. Liu, B. Hou, X. Xie, Insight into Cu_2O/CuO collaboration in the selective catalytic reduction of NO with NH_3: enhanced activity and synergistic mechanism, J. Catal. 384 (2020) 72–87.
[41] L. Qi, Z. Sun, Q. Tang, J. Wang, T. Huang, C. Sun, et al., Getting insight into the effect of CuO on red mud for the selective catalytic reduction of NO by NH_3, J. Hazard. Mater. 396 (2020) 122459.
[42] Q. Wang, H. Xu, W. Huang, Z. Pan, H. Zhou, Metal organic frameworks-assisted fabrication of CuO/Cu_2O for enhanced selective catalytic reduction of NOx by NH_3 at low temperatures, J. Hazard. Mater. 364 (2019) 499–508.
[43] Q. Sun, C. Zeng, M. Xing, B. Chen, D. Zhao, S. Hong, et al., Efficiently engineering Cu-based oxide by surface embedding of Ce for selective catalytic reduction of NO with NH_3, Nano 14 (06, 2019) 1950079.
[44] S.C. Yeo, S.S. Han, H.M. Lee, Mechanistic investigation of the catalytic decomposition of ammonia (NH_3) on an Fe (100) surface: a DFT study, J. Phys. Chem. C 118 (10, 2014) 5309–5316.
[45] K. Shojaee, B.S. Haynes, A. Montoya, The role of oxygen during the catalytic oxidation of ammonia on Co_3O_4(100), Appl. Surf. Sci. 316 (2014) 355–365.
[46] K. Shojaee, B.S. Haynes, A. Montoya, The catalytic oxidation of NH_3 on Co_3O_4(110): a theoretical study, P. Combust. Inst. 36 (3) (2017) 4365–4373.
[47] Y. Yang, J. Liu, Z. Wang, F. Liu, A skeletal reaction scheme for selective catalytic reduction of NOx with NH_3 over CeO_2/TiO_2 catalyst, Fuel Process. Technol. 174 (2018) 17–25.
[48] Y. Yang, J. Liu, F. Liu, Z. Wang, J. Ding, H. Huang, Reaction mechanism for NH_3-SCR of NOx over $CuMn_2O_4$ catalyst, Chem. Eng. J. 361 (2019) 578–587.
[49] D. Fang, D. Li, F. He, J. Xie, C. Xiong, Y. Chen, Experimental and DFT study of the adsorption and activation of NH_3 and NO on Mn-based spinels supported on TiO_2 catalysts for SCR of NOx, Comput. Mater. Sci. 160 (2019) 374–381.
[50] E. Gao, H. Pan, W. Zhang, Y. Li, G. Cao, M.T. Bernards, et al., Insights on the mechanism of enhanced selective catalytic reduction of NO with NH_3 over Zr-doped $MnCr_2O_4$: a combination of in situ DRIFTS and DFT, Chem. Eng. J. 386 (2020) 123956.

[51] J.P. Perdew, K. Burke, M. Ernzerhof, Generalized gradient approximation made simple, Phys. Rev. Lett. 77 (18, 1996) 3865–3868.
[52] M. Su, J. Cao, X. Tian, Y. Zhang, H. Zhao, Mechanism and kinetics of Cu_2O oxidation in chemical looping with oxygen uncoupling, P. Combust. Inst. 37 (2019) 4371–4378.
[53] C. Zheng, J. Cao, Y. Zhang, H. Zhao, Insight into the oxidation mechanism of a Cu-based oxygen carrier (Cu → Cu_2O → CuO) in chemical looping combustion, Energy Fuel 34 (7) (2020) 8718–8725.
[54] V. Massarotti, D. Capsoni, M. Bini, A. Altomare, A.G.G. Moliterni, X-ray powder diffraction ab initio structure solution of materials from solid state synthesis: the copper oxide case, Z. Kristallogr. 213 (5) (1998) 259–265.
[55] S. Sun, D. Zhang, C. Li, Y. Wang, Q. Yang, Density functional theory study of mercury adsorption and oxidation on CuO(111) surface, Chem. Eng. J. 258 (2014) 128–135.
[56] C. Zheng, H. Zhao, Exploring the microscopic reaction mechanism of H_2S and COS with CuO oxygen carrier in chemical looping combustion, Fuel Process. Technol. 205 (2020) 106431.
[57] C. Zheng, H. Zhao, Interaction mechanism among CO, H_2S and CuO oxygen carrier in chemical looping combustion: a density functional theory calculation study, P. Combust. Inst. (2020), https://doi.org/10.1016/j.proci.2020.06.260.
[58] F. Cao, S. Su, J. Xiang, L. Sun, S. Hu, Q. Zhao, et al., Density functional study of adsorption properties of NO and NH_3 over CuO/γ-Al_2O_3 catalyst, Appl. Surf. Sci. 261 (2012) 659–664.
[59] S. Sun, C. Li, D. Zhang, Y. Wang, Density functional theory study of the adsorption and dissociation of O_2 on CuO(111) surface, Appl. Surf. Sci. 333 (2015) 229–234.
[60] N.I. Il'chenko, G.I. Golodets, Catalytic oxidation of ammonia: I. reaction kinetics and mechanism, J. Catal. 39 (1) (1975) 57–72.
[61] Q. Imtiaz, D. Hosseini, C.R. Müller, Review of oxygen carriers for chemical looping with oxygen uncoupling (CLOU): thermodynamics, material development, and synthesis, Energ. Technol. 1 (11, 2013) 633–647.
[62] M. Zabilskiy, P. Djinović, E. Tchernychova, A. Pintar, N_2O decomposition over CuO/CeO_2 catalyst: new insights into reaction mechanism and inhibiting action of H_2O and NO by operando techniques, Appl. Catal. B-Environ. 197 (2016) 146–158.
[63] J. Sun, H. Chen, H. Wu, C. Zhou, H. Yang, Enhanced low-temperature selective catalytic reduction (SCR) of NOx by CuO-CeO_2-MnOx/γ-Al_2O_3 mixed oxide catalysts, Can. J. Chem. Eng. 97 (9) (2019) 2498–2504.
[64] J. Zhang, R. Zhang, B. Wang, L. Ling, Insight into the adsorption and dissociation of water over different CuO(111) surfaces: the effect of surface structures, Appl. Surf. Sci. 364 (2016) 758–768.
[65] X. Xiao, W. Qin, J. Wang, J. Li, C. Dong, Effect of surface Fe-S hybrid structure on the activity of the perfect and reduced α-Fe_2O_3(001) for chemical looping combustion, Appl. Surf. Sci. 440 (2018) 29–34.
[66] C. Lin, W. Qin, C. Dong, Reduction effect of α-Fe_2O_3 on carbon deposition and CO oxidation during chemical-looping combustion, Chem. Eng. J. 301 (2016) 257–265.